(Received 13 June 2024, Accepted 4 August 2024, Scheduled 18 August 2024)

Strip-Radiator and Reflector Based Multi-Layered CPW-Fed Antenna for Tracking Application

Trupti N. Pawase[1, 2], Anurag Mahajan[1, *], and Akshay Malhotra[3]

[1] *Symbiosis Institute of Technology, Symbiosis International (Deemed University), (SIU) Lavale, Pune, Maharashtra, India*
[2] *DES Pune University, Pune, Maharashtra, India*
[3] *Dr. Vishwanath Karad MIT World Peace University (MIT-WPU), Pune, Maharashtra, India*

ABSTRACT: This communication presents the design analysis and development of a compact, dual-band, circularly polarized, multilayer antenna for global positioning system (GPS), wireless local area network (WLAN), and Industrial Scientific, and Medical (ISM) applications. The antenna comprises two etched strip radiator and reflector layers on two Kapton substrates situated at a vertical distance of 18.47 mm. The inverted U-strip results in WLAN/ISM band from 2.30–2.62 GHz whereas the semi-circular arc-strip is responsible for generating the lower band from 1.46 to 1.73 GHz. The bottom surface reflector plane is applied below the main antenna radiator which results in a unidirectional radiation pattern with improved front-to-back ratio (FBR), antenna gain, radiation efficiency, and specific absorption rate (SAR). The reflector contains an inner square ring with a circular center ring. The reflection coefficient below -10 dB fractional bandwidth (FBW) is suitable for GPS/ISM/WLAN/Wi-Fi/Bluetooth etc operations. The maximum gain of 5.82 dBi is obtained at a frequency of 2.80 GHz. The antenna is designed on a flexible Kapton substrate of a size 28×31 mm^2. The SAR values below 0.01 W/kg and 0.02 W/kg are obtained at two resonance frequencies 1.60 GHz and 2.41 GHz, respectively. Therefore, the designed antenna is most suitable for indoor/outdoor wearable tracking purposes and also for medical applications.

1. INTRODUCTION

The importance of flexible and wearable electronics has greatly increased in recent years, especially in the development of advanced wireless communication systems [1–3]. These systems are getting more and more popular due to their adaptability in a wide range of situations, including residential, industrial, and military environments. In 2018, the worldwide market for flexible electronics had already exceeded 30 billion USD and expected to cross 300 billion USD in the next ten years [3, 4]. Furthermore, a primary obstacle for the next 5G network is to facilitate ubiquitous communication among devices while minimizing energy requirements. By 2020, projections indicated that the number of networked devices would surpass 50 billion, with each individual expected to connect to a minimum of ten gadgets [5]. These gadgets not only monitor vital signs but also assist in precisely determining the position of users in the field of health monitoring. Wearable technologies can greatly assist individuals with dementia who have a tendency to wander away from their residence. These devices enable caretakers to monitor and track the patients, ensuring their safety in both indoor and outdoor settings. A key system that relies on satellites to deliver precise positioning and timing data, especially for outdoor environments, is Global Navigation Satellite System (GNSS) [6].

GNSS-enabled devices are mainly important in surveying, military operations, car navigation, and health and activity monitoring systems. These devices are commonly embedded in everyday items like smartphones, tablets, and cameras, and increasingly in wearable technology like smart watches and collars [6].

Due to their proximity to the human body, it is crucial to study their impact in the reactive near-field region at lower frequencies. One significant limitation of GNSS-enabled devices is their poor signal penetration indoors, which reduces their effectiveness inside buildings. To overcome this challenge, there is a strong need to develop a versatile and flexible wearable system capable of functioning effectively in diverse settings, both indoors and outdoors. The optimal system would reduce the impact of body coupling, integrate different types of antennas into a sleek, conformal design, and operate with minimal interference from the closeness of the human body [7].

Indoor location tracking systems often rely on WLAN technology, which uses linearly polarized antennas. These antennas are favored for their straightforward design and effectiveness in ensuring reliable communication links. The WLAN signals' ability to precisely track users' movement both indoors and outdoors emphasizes the need for wearable devices that can handle both linear and circular polarizations.

Wearable and flexible antennas differ from traditional rigid patch antennas in several ways. The impact of such wearable antennas on human tissue, such as the specific absorption rate, must be considered.

The literature uses a variety of metamaterials for SAR reduction, including frequency selective surface (FSS), artificial magnetic conductor (AMC), and electromagnetic band gap (EBG) [8].

* Corresponding author: Anurag Mahajan (anurag.mahajan@sitpune.edu.in).

Abirami and Sundarsingh have proposed a replacement of the conventional Yagi-Uda antenna into polyester film based flexible planar form by using an electromagnetic band gap (EBG)-backed printed antenna for on-body communication at 2.4 GHz with increased gain and improved specific absorption rate (SAR) 0.07 W/kg [12].

Velan et al. have proposed a dual-band square-slotted EBG antenna for wearable applications. The antenna covers GSM-1800 MHz and ISM 2.45 GHz bands. The monopole fractal-based antenna was fabricated on jeans material, and SARs were validated which were 0.02 and 0.01 W/kg for dual bands [13].

Zhang et al. have proposed a dual-band pinwheel-shaped (Spiral slot patch) slotted EBG antenna for C-band applications. The antenna has low radiation efficiency while the realized gain is enhanced by 1.87 dB and 1.56 dB at 4.57 GHz and 5.06 GHz. The proposed EBG structure also helps to improve impedance bandwidth, radiation efficiency, and gain of the antenna [14]. Yan et al. have designed and developed an artificial magnetic conductor (AMC) based dual-band textile antenna for WLAN application, which can operate in 2.4 GHz as well as in 5 GHz band. The first 2.4 GHz resonant frequency band is achieved by a rectangular patch while on the other hand, the second 5 GHz resonant frequency band is achieved by a patch-etched slot dipole. The antenna has been measured in free space and near the human body and generates satisfactory results in terms of its resultant parameters like SAR, gain, and radiation patterns [15].

Paracha et al. have proposed a dual-polarized differentially fed complementary split ring resonator (CSRR) and U-slot loaded wearable antenna for dual-band operation. The circular polarization in the GNSS L1/E1 lowers the 1.57 GHz band by introducing a CSRR on the antenna patch. The upper 2.45 GHz WLAN band is achieved by etching a U-slot in the bottom ground. The radiation pattern has been made unidirectional by introducing an AMC reflector surface [16].

Joshi et al. have presented a double-layered dual-band wearable textile antenna for GPS, wireless body area network (WBAN), and WLAN bands operations. The antenna gain enhancement and radiation back lobe elimination are carried out by introducing a 3×3 AMC structure as a reflector below the radiator patch. Truncated square patches and rectangular slits at four corners have been used to achieve dual bands and dual polarizations. This structure gives 0.12 W/kg SAR with front to back ratio (FBR) above 10 dB [17].

Rojhani et al. have demonstrated a circularly polarized CPW-fed slot antenna with excellent performance parameters for the use of GPS at the 1.575 GHz band. The antenna radiator is fed by a 50 Ω, L-shaped CPW feed that generates circular polarization. On the bottom ground, two metal-defected square rings are slotted to achieve impedance bandwidth [18].

Yuan et al. have discovered a wideband GNSS antenna for emergency communications such as inshore fishery, emergency rescue, and forest fire prevention. The CPW-fed antenna radiator works with the modified reflector to make the antenna radiation unidirectional for GNSS application, in which the gap between the radiator and the reflector has been reduced to improve impedance bandwidth (IBW) and axial ratio bandwidth (ARBW) [19]. The limitation of this design is that it is not flexible, but FR4 substrate is used, and no analysis about SAR is given.

Mishra et al. have proposed a CPW-fed planar circular polarization (CP) antenna for tri-GPS bands L1 (1575 MHz), L2 (1227 MHz), and L5 (1176 MHz). The circular polarization is the result of appending a $\lambda/4$ long arc with inset feed and cutting two slits into the elliptical patch. The proposed antenna fulfills the necessary conditions in all 3 bands of GPS except the rigid substrate RT Duroid 5880, and SAR analysis is not done [20].

Singh et al. have described the design, fabrication, and measurements of a compact FR4 based dual-band antenna for ISM/wearable operations. The SAR results are within the approved standards, but it is not a flexible antenna [21]. Gundapaneni et al. have presented an inverted-Ω shape connected with a fork-shaped stub monopole antenna for ISM band/wearable application on 1.27 mm thickness Roger's 3006 substrates, and SAR values are coming within the standards, i.e., 0.45 W/kg for flat and 0.53 W/kg for bent cases [22].

However, most dual-band designs in the literature have a textile based substrate [12–14] or rigid substrate [19–22], low FBR [15], huge in size [14, 15], and no proper synthesis on SAR is given. Textile antennas coupled with EBG structures are reported in [14]. In order to get over these restrictions, it is crucial to choose a flexible substrate carefully.

The ensuing difference in dimensions is a common issue brought on by stretching and compression in a structure made of fabrics. Variations in dimensions have a significant impact on the electromagnetic properties of the antennas [1–3]. The electrical characterization of paper is a crucial aspect for paper-based flexible antennas, because it is influenced by environmental conditions like as humidity. Kapton was selected as the antenna substrate due to its superior combination of electrical and physical properties, as well as its low loss tangent [4].

The proposed work is novel as in multi-layer antenna multiple-strip radiator technology has been utilized as an alternative to the rectangular or circular patch to achieve the dual-band nature of the antenna reflection coefficients [8–11]. A reflector surface is used at a suitable distance from the radiating patch to make the bidirectional radiation pattern unidirectional pattern (necessary condition) for the use of an antenna in a GPS band. The primary objective of this design is to achieve a GPS band with acceptable performance parameters by the use of a semi-circular arc-strip, and the secondary aim of this research is to achieve an upper band for WLAN and ISM band applications by the use of a U-strip radiator.

2. ANTENNA CONFIGURATION

2.1. Antenna Geometry

A multi-layer antenna has been proposed. The proposed antenna consists of two Kapton substrates (permittivity 3.4 and thickness 1.53 mm) of a compact size of 28 mm × 31 mm each. The antenna was designed at a frequency of 2.45 GHz. The top layer of the first substrate is used as a radiator and CPW

TABLE 1. Antenna dimensional descriptions.

Designation	Dimensional Parameter	Value (in mm)
Kapton Dielectric Substrate Permittivity	ε_r	3.4
Substrate Length	L_{sub}	31
Substrate Width	W_{sub}	28
Substrate Height	h	1.53
CPW Ground Length	L_{CPW}	12.7
CPW Ground Width	W_{CPW}	4.0
CPW Ground Gap	G_{CPW}	2.6
Feed Width	W_{f}	1.8
Feed Length	L_{f}	9.2
I$^{\text{st}}$ Strip section Length	L_{strip1}	10.3
II$^{\text{nd}}$ Strip section Length	L_{strip2}	4.15
III$^{\text{rd}}$ Strip section Length	L_{strip3}	9.5
Each Strip section's Width	W_{strip}	0.5
Outer Half Circle Arc Radius	R	11
Inner Half Circle Arc Radius	$R - W_{\text{strip}}$	10.5
Port Length	L_{Port}	8.0
Inner Conductor Radius	R_{i}	0.7173
Outer Conductor Radius	R_0	2.4
Reflector Substrate Length	L_{sub}	31
Reflector Substrate Width	W_{sub}	28
Reflector Substrate Height	h	1.53
Outer Dimensions of Square Reflector	$L_{\text{ref}} \times W_{\text{ref}}$	12×12
Inner Dimensions of Square Reflector	$L \times W$	11×11
Outer Radius of Ring Reflector	R_2	11.5
Inner Radius of Ring Reflector	R_1	11
The gap in Rectangular or Circular Strip	W_{strip}	0.5
The gap between the two Substrates	G	18.47
The gap between the reflector and Radiator	$G + h$	20

feed while the top of the second Kapton substrate is used as a reflector. The integration of U-strip and semi-circular arc strips with a modified reflector forms a new compact 3-D multi-layered antenna that has a unidirectional radiation pattern. The antenna resonates at 2.41 GHz when inverted U-strip of thickness (W_{strip}) is 0.5 mm, and the total length of inverted U-strip (L_{strip}) is 23.85 mm.

The total inverted U-strip length

$$L_{\text{strip}} = L_{\text{strip1}} + L_{\text{strip2}} + L_{\text{strip3}} \tag{1}$$

The resonance frequency is evaluated by using the following relation [23]

$$f_{2.41\text{ GHz}} = \frac{c}{4L_{\text{strip}}\sqrt{\varepsilon_{\text{reff}}}} \tag{2}$$

c = Velocity of light, $\varepsilon_{\text{reff}}$ = Effective permittivity [8–10]

$$\varepsilon_{\text{reff}} = \frac{\varepsilon_{r+1}}{2} + \frac{\varepsilon_{r-1}}{2}\left[\frac{1}{\sqrt{1+\frac{12h}{w}}} + 0.04\left(1 - \left(\frac{W_{\text{strip}}}{h}\right)\right)^2\right] \tag{3}$$

h = height of the substrate (1.53 mm).

As c and ε_r are fixed for the Kapton substrate therefore the resonance frequency value is tuned by adjusting the value of the thickness/width of the strip and length of three-strip sections of the inverted U-strip line. The total U-strip evaluated length value using Equation (2) is 20 mm, and the simulated optimized value is 23.85 mm.

A semi-circular arc strip of thickness 0.5 mm and total periphery of electrical length 33.656 mm (simulated arc circumference C) was used, then the antenna resonates at a frequency of 1.60 GHz. Here, resonance frequency can be tuned by varying the radius of the outer semi-circular strip and the width of the strip.

The total semi-circular arc-strip circumference length

$$C = \pi(R - w_{\text{strip}}) \tag{4}$$

R = Outer half circle arc radius

The resonance frequency is evaluated using the following equation.

$$f_{1.60\text{ GHz}} = \frac{c}{4C\sqrt{\varepsilon_{\text{reff}}}} \tag{5}$$

The evaluated value of the inner radius of the circular arc strip was 9.84 mm whereas the simulated optimized value is 10.50 mm.

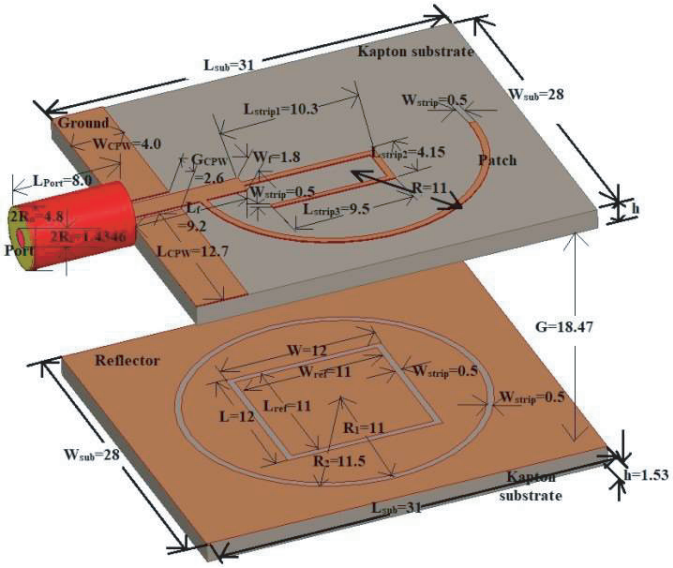

FIGURE 1. Antenna geometrical dimensions (in mm).

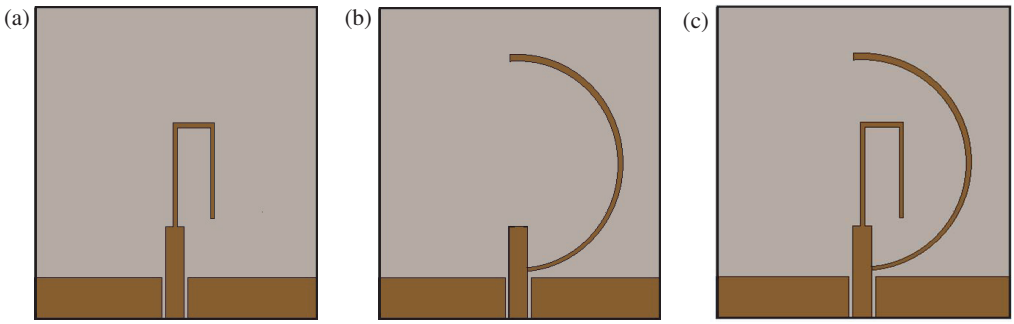

FIGURE 2. Effect of adding reflector surface. (a) U-strip in patch. (b) Semicircular strip in patch. (c) U-strip and semicircular-strip patch.

This inverted U strip structure along with semicircular arc attached with 50 Ω feed makes the antenna result in dual bands at 2.41 GHz and 1.60 GHz with acceptable reflection coefficient. A reflector plane is used below the antenna radiator substrate at a separation of 20 mm from the radiator patch for perfect working of the antenna for GPS tracking. A square ring of arm's length 12 mm and a circular ring of outer radius 11.5 mm slots are used in the bottom reflector plane. These will result in improved reflection coefficient values. A 50 Ω SMA connector is connected at the 50 Ω feed line along with a coplanar waveguide (CPW) for the excitation of the antenna radiator [10]. The proposed GPS tracking antenna configuration is represented in Figure 1, and all the measurements of simulated design dimensions units with the physical meaning of the dimensional parameters are represented in Table 1. All dimensions are measured in millimeters (mm).

2.2. Antenna Development

The proposed CPW-fed antenna comprises a radiator and reflector. The forthcoming subsection explains the effect of the development of the radiator as well as the effect of the addition of a reflector.

2.2.1. Antenna Radiator

The antenna radiator is developed by first attaching an inverted U-strip arm and then attaching a semicircular arc arm in the feed line.

The effect of individual attachment of U-strip and semicircular arc-strip in radiating patch and their combined effects are displayed in Table 2. The radiator step-by-step development is shown in Figures 2(a)–(c), and their effect on reflection coefficient plots is compared in Figure 3. It is observed from Figure 3 that an inverted U-strip and a semi-circular arc-strip improve impedance matching and the reflection coefficient below −10 dB level. It also provides acceptable gain with a bidirectional radiation pattern.

2.2.2. Antenna Reflector

The radiator of the antenna is loaded by a full surface reflector at a separation of 20 mm as represented in Figure 4(a). The reflector layer is further loaded with square ring and circular ring slots as displayed in Figures 4(b)–(d).

The effects of reflector loading with an individual square ring of arm's length 12 mm and a circular ring of radius

TABLE 2. Effect of reflecting stages.

Mode	f_r (GHz)	S_{11} (dB)	−10 dB BW (GHz)	FBW (%)	Gain (dBi)
With U-Patch	2.42	−11.23	2.33–2.51	7.44	3.87
With Semi circular-Patch	1.73	−31.90	1.57–1.92	20.23	0.49
With U-strip and Semi circular-Patch	1.66	−24.27	1.52–1.78	15.66	0.02
	2.47	−14.32	2.35–2.68	13.36	3.81

TABLE 3. Effect of adding a reflector.

Reflector Modes	f_r (GHz)	S_{11} (dB)	−10 dB BW(GHz)	FBW (%)	Gain (dBi)
Full surface	1.60	−26.78	1.46–1.72	16.25	−0.54
28 mm × 31 mm	2.42	−10.87	2.36–2.50	5.78	4.99
Full surface with	1.60	−35.0	1.45–1.73	17.5	−0.21
circular Ring Cut	2.41	−13.60	2.31–2.59	11.62	5.06
Full surface with square Cut	1.61	−26.06	1.48–1.74	16.14	−0.40
	2.41	−11.20	2.35–2.51	6.61	5.24
Full surface with square	1.60	−50.14	1.46–1.73	16.87	0.05
plus circular Ring Cut	2.41	−14.70	2.30–2.62	13.23	5.06

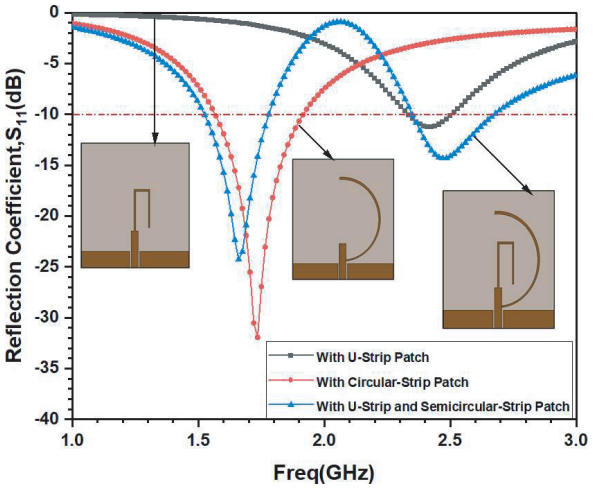

FIGURE 3. Effect of adding a reflector surface.

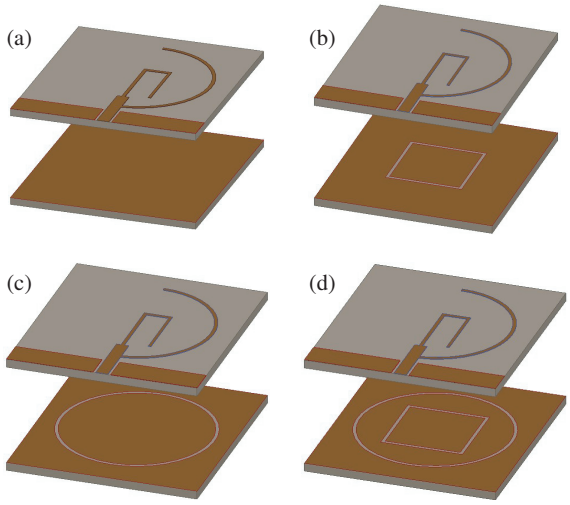

FIGURE 4. Antenna reflector mode. (a) Antenna with full surface reflector. (b) Antenna with square ring cut reflector. (c) Antenna with circular ring cut reflector. (d) Antenna with square plus circular square ring cut reflector.

11.5 mm are illustrated in Figure 5. Finally, the combination of square plus circular ring reflector structure is used with radiator which results in an excellent impedance match at 2.41 GHz and 1.60 GHz with acceptable gain and bandwidth as discussed in Table 3.

3. RESULTS AND DISCUSSIONS

3.1. Summarized Results

The proposed wearable GPS tracking antennas with a reflector and without a reflector have been summarized in terms of their performance parameters in Table 4. All these resultant parameters are explained in detail in the succeeding sections.

3.2. Antenna Reflection Coefficient

The final antenna structure with inverted U-strip and semi-circular-arc simulated and antenna results are analyzed and displayed in Figure 6. This structure consists of a multilayer structure separated by a 20 mm distance between antenna radiator and the reflector. When the reflector loaded case is compared to the case without reflector it has been recorded that the reflector improves all the antenna performance parameters like reflection coefficients, FBW, and gain at resonant frequencies as mentioned in Table 4.

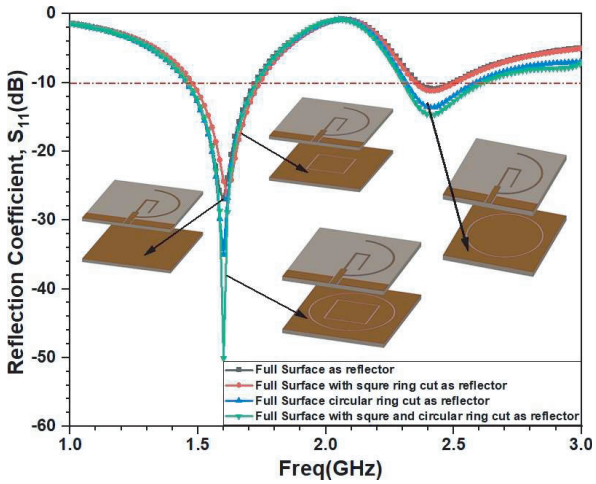

FIGURE 5. Reflection coefficient with a reflector.

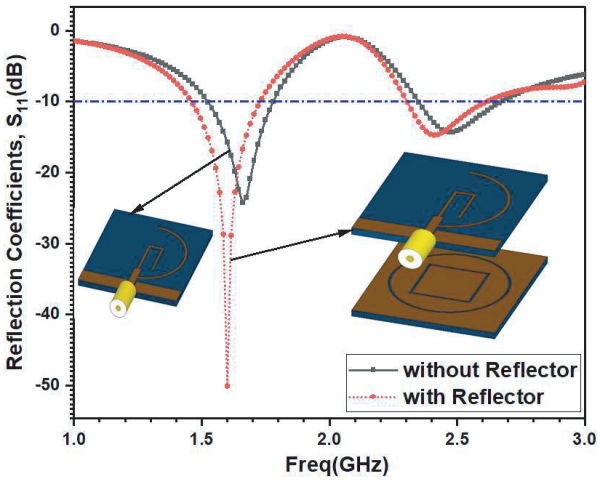

FIGURE 6. Reflection coefficient.

TABLE 4. Summary of results.

Antenna Parameters	Without Reflector	With Reflector
Reson. Freq. f_r (GHz)	1.66, 2.47	1.60, 2.41
Ref. Coeff. S_{11} (dB)	-24.27, -14.32	-50.14, -14.70
-10 dB BW (GHz)	(1.52–1.78), (2.35–2.68)	(1.46–1.73), (2.30–2.62)
FBW (%)	15.66, 13.36	16.87, 13.23
Gain (dBi)	0.02, 3.81	0.05, 5.06
Axial ratio (AR)	< 3 dB	< 3 dB
VSWR (< 2)/ IBW (GHz)	(1.51–1.79), (2.34–2.70)	(1.45–1.74), (2.30–2.64)
Radiation pattern	Bi-directional	Uni-directional
Rad. Efficiency (%)	109.01, 99.74	105.20, 99.15
Maximum SAR (W/kg)	< 0.5, < 0.5	< 0.01, < 0.02

Comparative analysis of the reflection coefficients for structures with and without reflectors reveals significant improvements. Specifically, the structures with reflectors demonstrate reflection coefficients of -50.14 dB and -14.70 dB, compared to -24.27 dB and -14.32 dB for those without reflectors in the lower and upper band frequencies, respectively, as illustrated in Figure 6.

3.3. VSWR

The voltage standing wave ratio (VSWR) of the proposed GPS tracking antenna is plotted against that without reflector antenna as shown in Figure 7. The lowest value close to 1 has been achieved at a frequency of 1.60 GHz with a reflector antenna as displayed in Figure 7. The dual bands with VSWR lower than 2 have excellent impedance matching in the impedance bandwidth (1.45–1.74) GHz and (2.30–2.64) GHz. The corresponding resonance frequencies within this bandwidth are most suitable for GPS and ISM/WLAN applications.

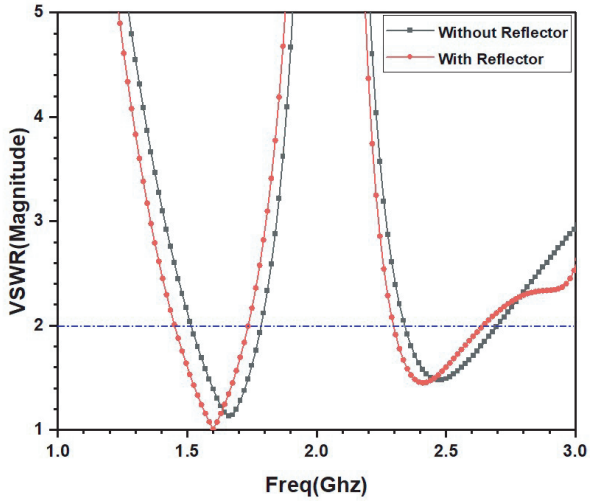

FIGURE 7. VSWR plots.

The VSWR is a critical measure of how efficiently a radio frequency power is transmitted from a power source to a load, with lower values indicating better matching and reduced signal reflections. The VSWR analysis shows significant improvements in VSWR when reflectors are included. Specifically, for the lower band, the VSWR improves from 1.51 to 1.79 without reflectors to 1.45 to 1.74 with reflectors. Similarly, in the upper band, the VSWR improves from 2.34 to 2.70 without reflectors to 2.30 to 2.64 with reflectors, demonstrating enhanced transmission efficiency and reduced loss.

3.4. Electric Field Vector

The electric field vector magnitude of the GPS tracking antenna has been evaluated at resonance frequencies 1.60 GHz and 2.41 GHz and illustrated in Figures 8(a)–(b). The figures show that the electric field magnitude of the dual-band radiating patch is maximum at the feed line and the near region of the CPW ground around the feed. The highest electric field is found on the U-strip while the medium field magnitude exists

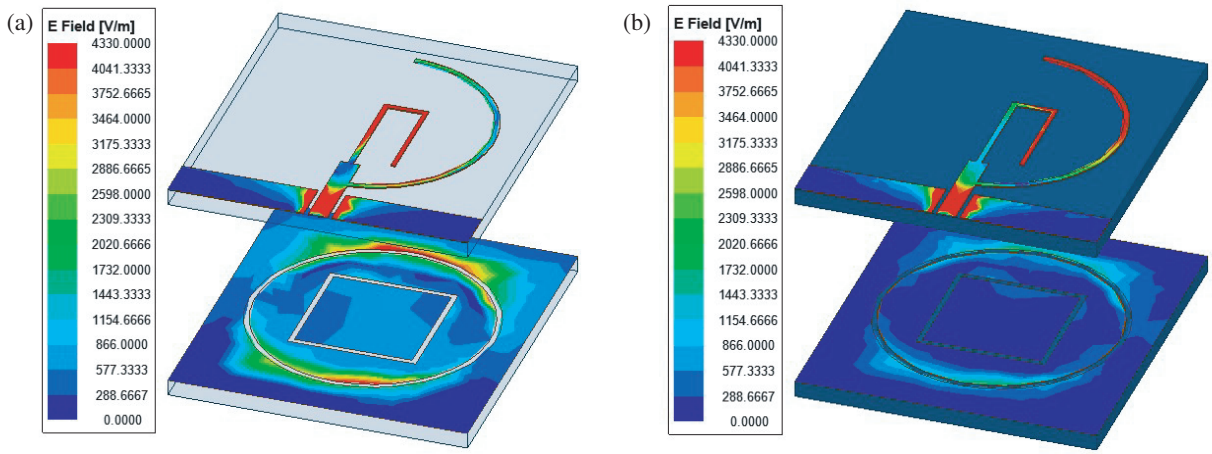

FIGURE 8. Electric field vector. (a) At 2.41 GHz. (b) At 1.60 GHz.

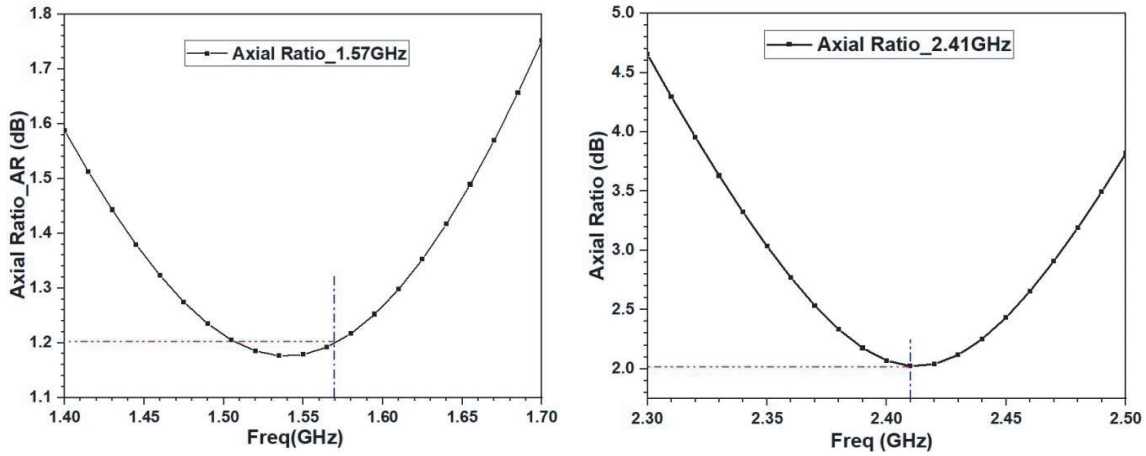

(a) (b)

FIGURE 9. Axial ratio. (a) 1.57 GHz. (b) 2.41 GHz.

in the semi-circular arc-arm strip. The minimum at the reflector plane center and the corner of the reflector plane at 2.41 GHz is displayed in Figure 8(a). On the other hand at lower resonance frequencies, the electric field vector is the highest at the open ends of the U-strip and semi-circular arc-arm strips.

3.5. Axial Ratio

The axial ratio (AR) plots of the antenna with reflector and without reflectors are compared in Figure 9. It is observed from the AR plot that AR is less than 3 dB in the whole frequency range for both cases. This strongly implies that the antenna is circularly polarized.

3.6. Radiation Pattern

The E-plane and H-plane gain radiation polar plots of the proposed antenna at the two resonance frequencies 1.60 and 2.41 GHz are plotted in Figure 10 and Figure 11. The red line with a square symbol represents the antenna without a reflector plot while the blue line with circle symbols represents the pattern of the antenna with a reflector. The antenna, both with and without a reflector, demonstrates a bi-directional E-plane pattern resembling the shape of a figure-eight ('8'). When the back reflector is applied on the radiating patch, the H-pattern becomes unidirectional as it is the desired condition in case the antenna is used for GPS purposes. Therefore, front to back ratio (FBR) goes high as displayed in Figure 11.

The three-dimensional (3D) radiation patterns of the proposed multi-layered antenna are showcased in Figures 12(a)–(b) at resonant frequencies of 1.60 GHz and 2.41 GHz. These visualizations offer a comprehensive perspective of the antenna's radiation across horizontal, vertical, and other planes. Notably, the patterns reveal that radiation is maximal in the E-plane in one direction and minimal in the opposing direction. This characteristic underscores the excellent front-to-back ratio exhibited by the proposed antenna.

3.7. Specific Absorption Rate (SAR)

The SARs of the two cases with and without a reflector at resonance frequencies 1.60 GHz and 2.41 GHz are illustrated in Figures 13(a)–(d). In the first two cases, the SAR value is below 0.5 W/kg. On the other hand, when the reflector surface

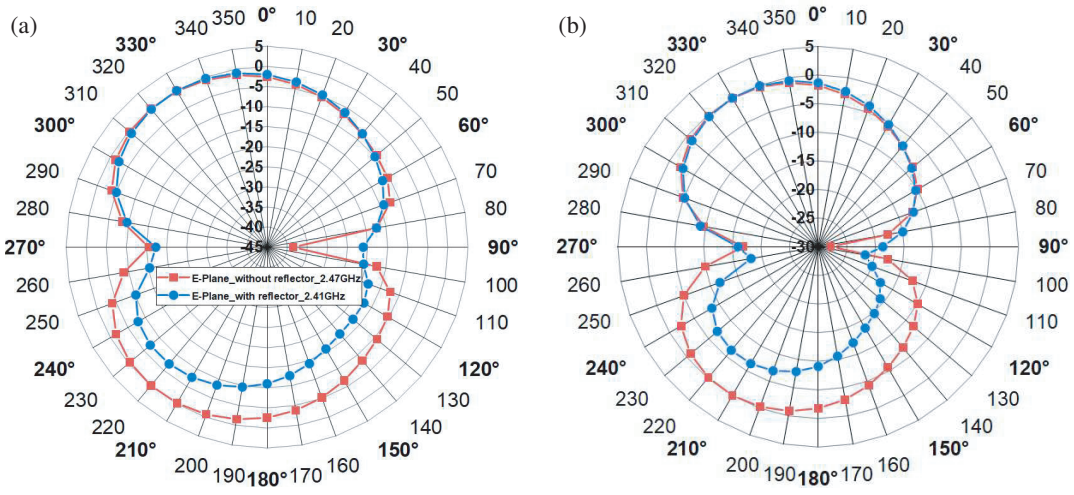

FIGURE 10. E-plane radiation pattern. (a) E-plane patterns at 2.4 GHz. (b) E-plane patterns at 1.60 GHz.

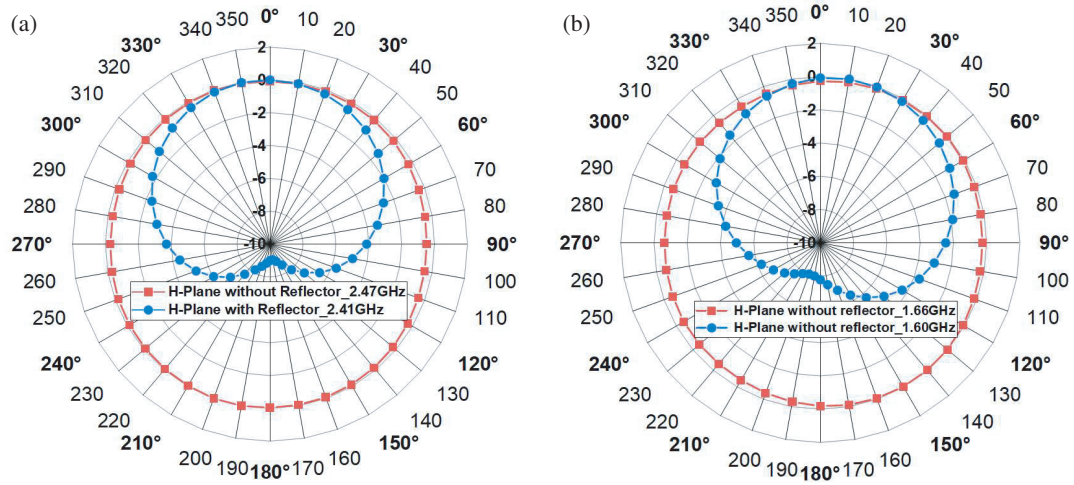

FIGURE 11. H-plane radiation pattern. (a) H-plane patterns at 2.41 GHz. (b) H-plane patterns at 1.60 GHz.

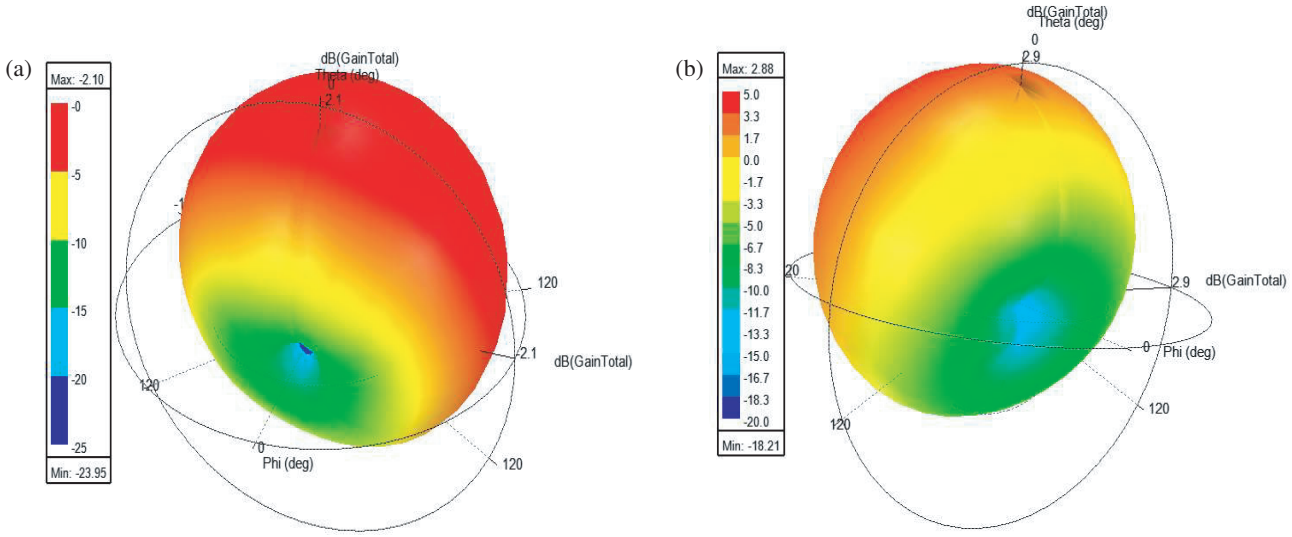

FIGURE 12. 3D-radiation pattern. (a) At 1.60 GHz. (b) At 2.41 GHz.

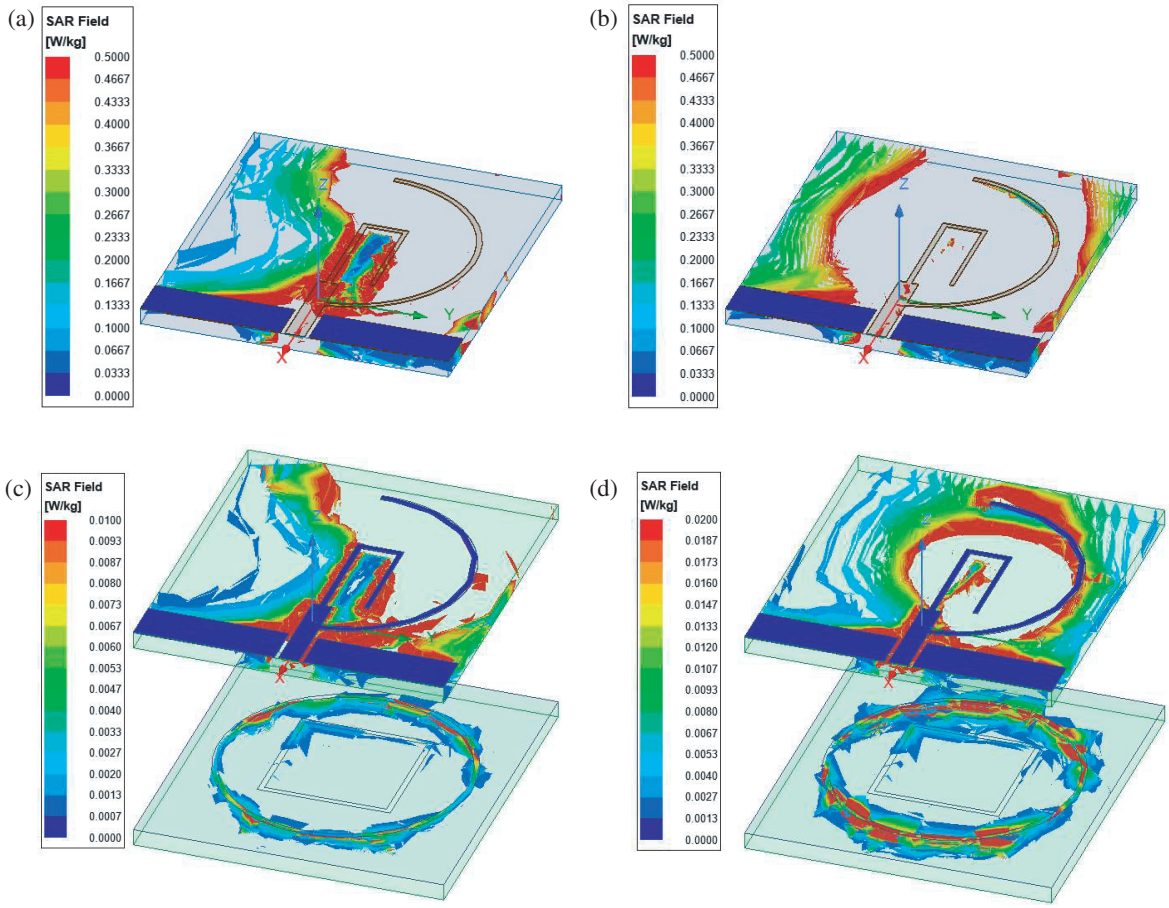

FIGURE 13. Specific absorption rate plot. (a) At 1.6 GHz without a reflector. (b) At 2.41 GHz without a reflector. (c) At 1.6 GHz with a reflector. (d) At 2.41 GHz with a reflector.

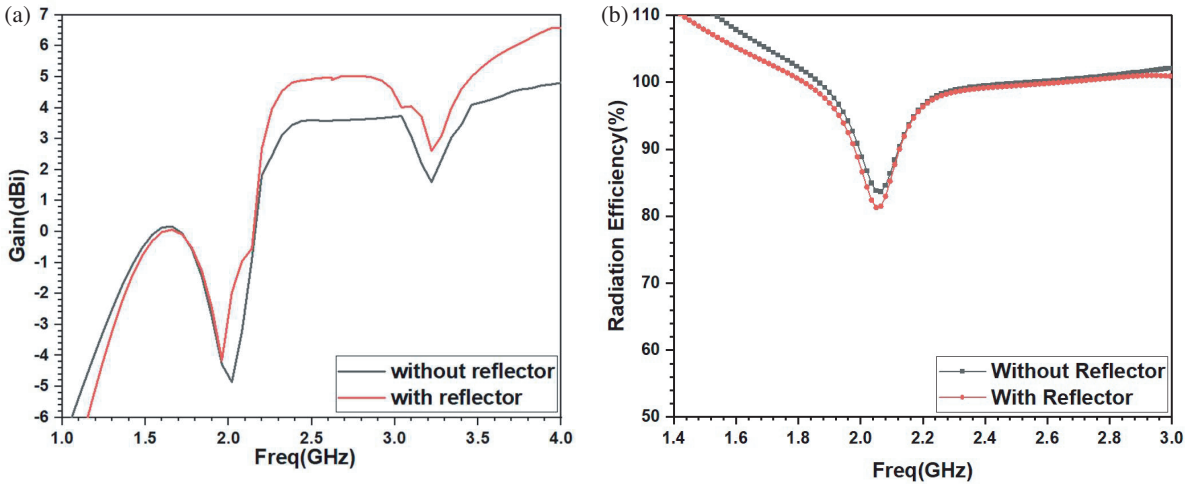

FIGURE 14. Gain and radiation efficiency plots. (a) Gain plot. (b) Efficiency plot.

is applied, SAR value is extremely improved to 0.01 W/kg and 0.02 W/kg, which is well below the government-specified standard SAR (1.6 W/kg) value. It is observed that the maximum value of SAR is near the U-strip of the radiator when the antenna is loaded with a reflector.

3.8. Gain and Radiation Efficiency

The gain and radiation efficiency plots of the proposed GPS tracking antenna are displayed in Figures 14(a)–(b). The highest gain 5.82 dBi is obtained at a frequency of 2.80 GHz, and the minimum radiation efficiency of 80.2% is obtained at a fre-

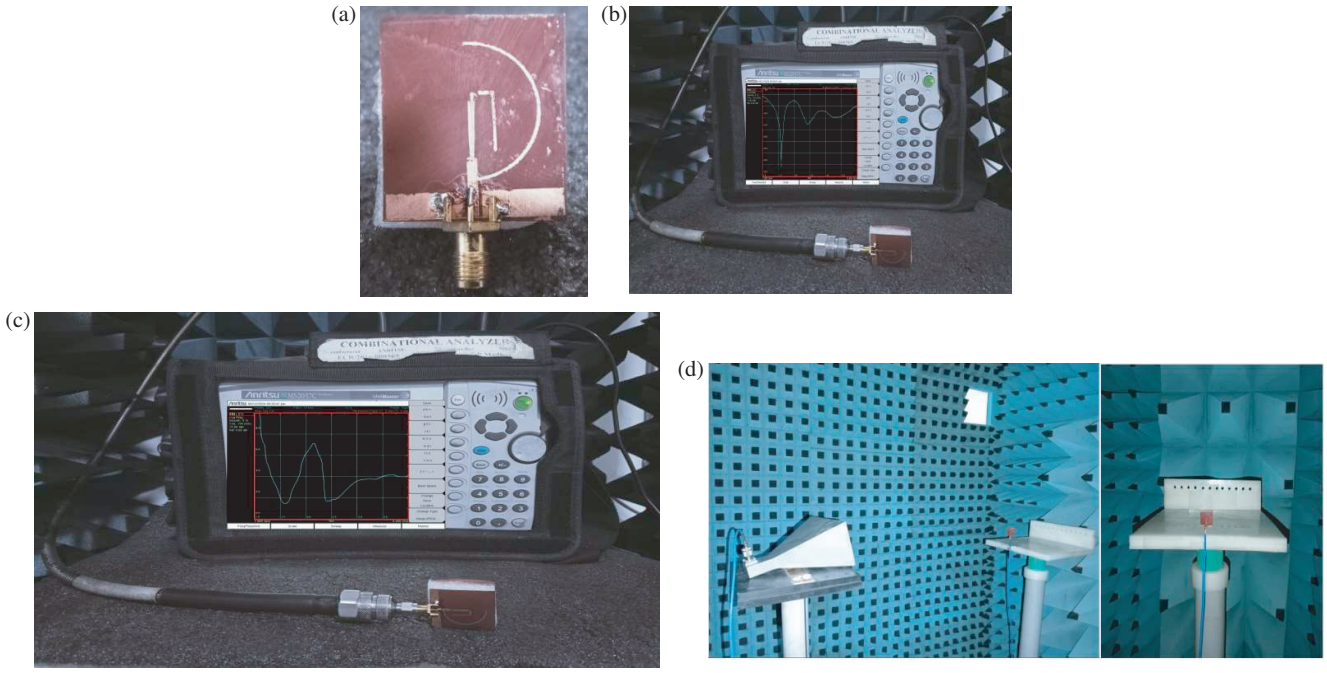

FIGURE 15. Antenna fabrication and measurements. (a) Fabricated front view of proposed antenna. (b) Measured reflection coefficient of antenna VNA. (c) Measured VSWR of antenna VNA. (d) Anechoic chamber testing of proposed antenna.

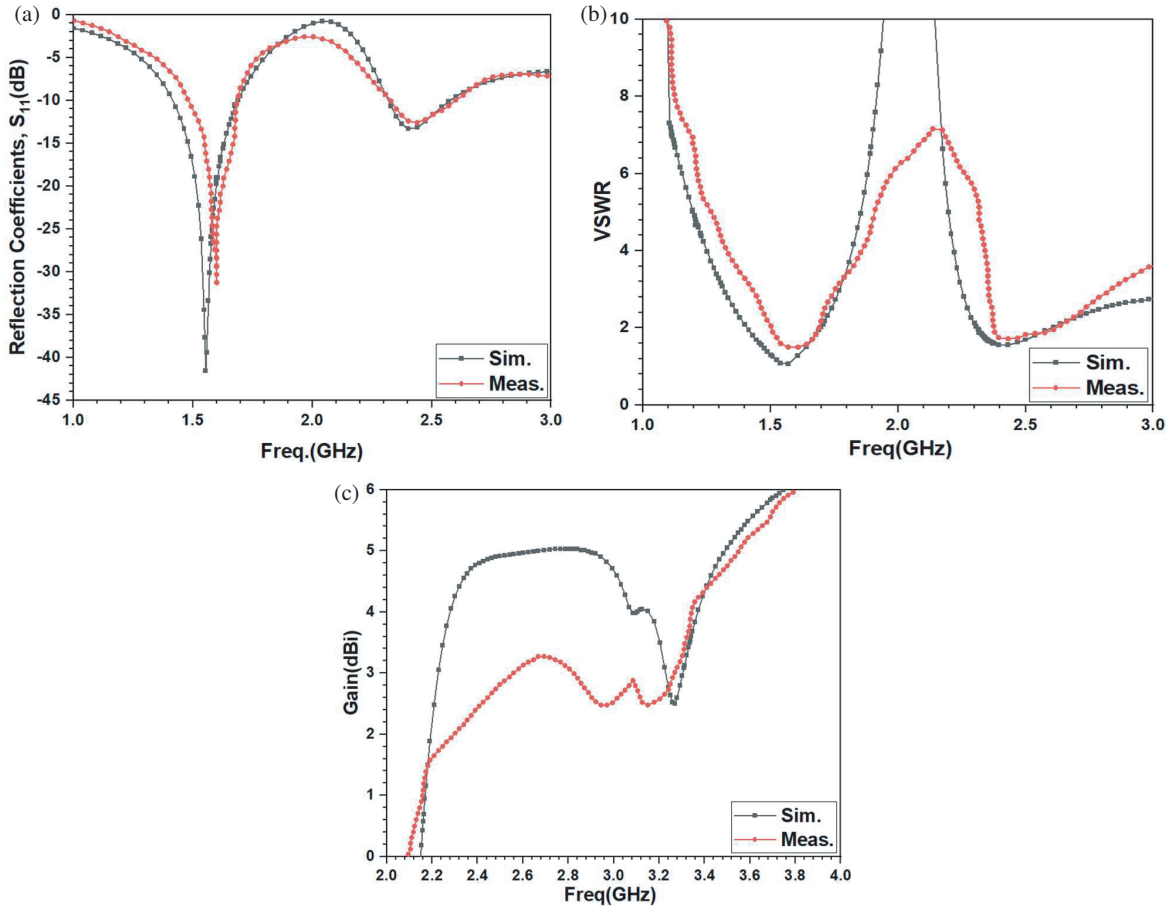

FIGURE 16. (a) Comparison of measured and simulated return losses. (b) Comparison of measured and simulated VSWRs. (c) Measured and simulated gain comparison.

TABLE 5. Comparison with similar antennas in the literature.

Ref. No. (Appl.)	Sub. used	G (dBi)	Ant. Size (mm^3)	BW (GHz)	SAR (W/kg)
[12] 2017 (ISM/WLAN band)	Polyester Sheet $\varepsilon_r = 1.03$ $h = 0.0625$ mm $\tan\delta = 0.045$	8.5	$135 \times 135 \times 6.0$	(2.3–2.75)	< 0.0698
[13] 2015 (GPS/ WLAN)	Jean fabric $\varepsilon_r = 1.7$ $h = 1.0$ mm $\tan\delta = 0.085$	2.5, 1.5	$150 \times 150 \times 2.0$	(1.78–1.98), (2.38–2.51)	< 0.024, < 0.016
[14] 2015 (C-Band)	FR4 $\varepsilon_r = 4.4$ $h = 1.6$ mm $\tan\delta = 0.02$	1.87, 1.56	$60 \times 60 \times 2.0$	(4.43–4.56), (4.96–5.01)	NA
[15] 2014 (WLAN/WBAN)	Felt $\varepsilon_r = 1.44$ $h = 3.0$ mm $\tan\delta = 0.044$	2.4, 4.0	$100 \times 100 \times 3.0$	(2.4–2.484), (5.15–5.85)	< 0.468 < 0.03
[18] 2018 (GPS)	FR4 $\varepsilon_r = 4.4$ $h = 0.8$ mm $\tan\delta = 0.02$	-1.75	$56 \times 56 \times 0.8$	(1.525–1.6),	NA
[19] 2019 (GNSS/GPS)	FR4 $\varepsilon_r = 4.4$ $h = 0.8$ mm $\tan\delta = 0.02$	5.87	$65.5 \times 65.5 \times 13$	(1.53–2.28)	NA
[20] 2019 (GPS)	RT Duroid 5880 $\varepsilon_r = 2.2$ $h = 3.175$ mm $\tan\delta = 0.0009$	4.39, 5.94	$172.37 \times 96.38 \times 3.175$	(1.123–1.254), (1.565–1.585)	NA
[24] 2017 (WLAN/WBAN)	*Felt $\varepsilon_r = 1.44$ $h = 3.0$ mm $\tan\delta = 0.044$ *PDMS $\varepsilon_r = 2.7$ $h = 3.0$ mm $\tan\delta = 0.0137$	NA	$90 \times 90 \times 6.51$ $141 \times 147 \times 6.035$	(2.38–2.48), (5.26–6.1) (2.39–2.61), (5.62–5.90)	< 0.11 < 0.043
[25] (2020) (WLAN/Wi-MAX/ Bluetooth)	FR4 $\varepsilon_r = 4.4$ $h = 1.6$ mm $\tan\delta = 0.02$	2.30	$23 \times 23 \times 1.6$	2.0–2.60, 3.28–3.7, 4.8–6.5	NA
[26] 2024 (GNSSs	FR4 $\varepsilon_r = 4.4$, $h = 3$ mm $\tan\delta = 0.02$	3.5	$\pi \times 50 \times 50 \times 4$	1.561 1.575	NA
Prop. Work (GPS/WLAN)	Kapton $\varepsilon_r = 3.4$ $h = 1.53$ mm $\tan\delta = 0.02$	0.05, 5.06	$31 \times 28 \times 1.53$	(1.46–1.73), (2.30–2.62)	< 0.01 < 0.02

Note: Appl. = Application; Sub. = Substrate; NA = Not Available; Prop. = Proposed

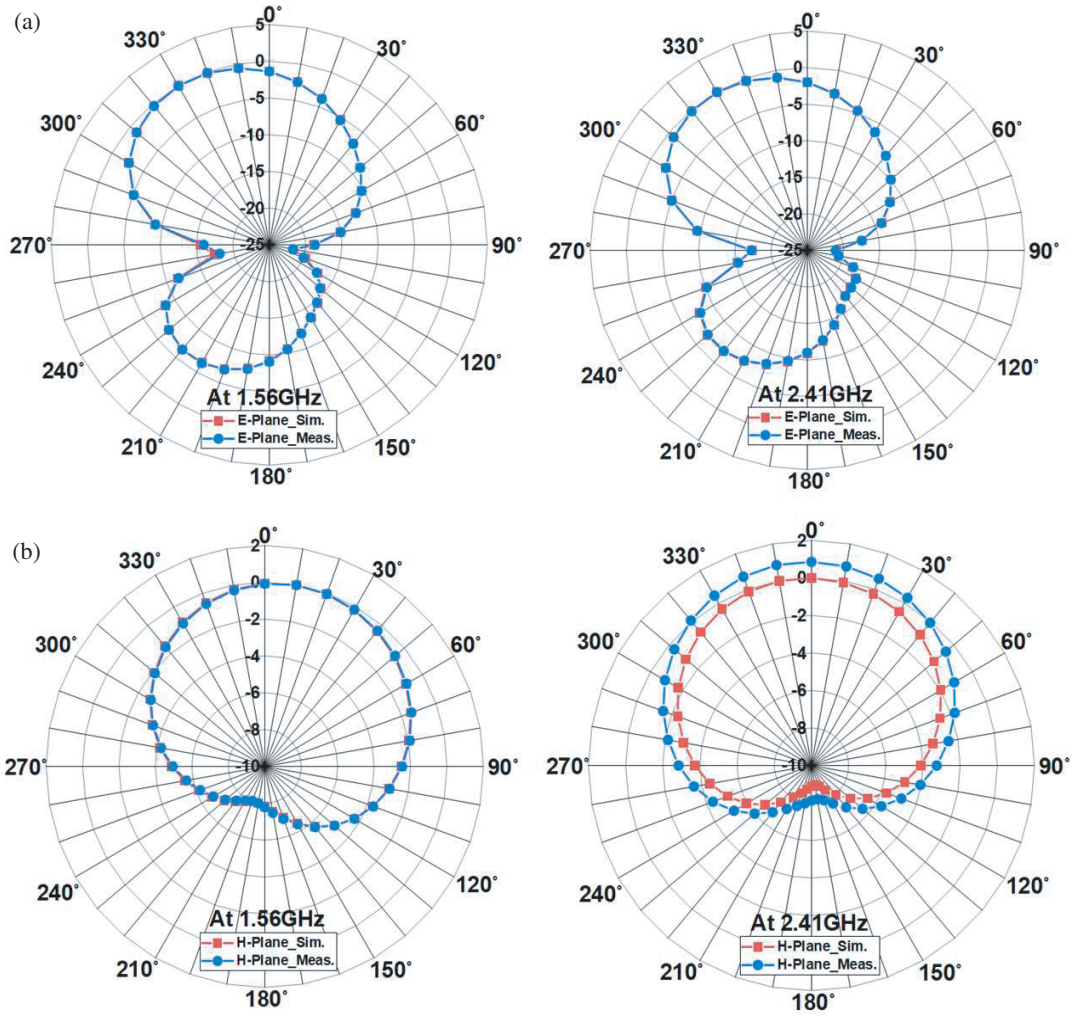

FIGURE 17. Measured and simulated radiation patterns in E and H planes. (a) E-plane at 1.56 GHz. (b) H-plane at 2.41 GHz.

quency of 2.10 GHz with a gain value of 3.25 dBi. The radiation efficiency is obtained at a frequency of 2.41 GHz.

The gain and radiation efficiency plots of the proposed GPS tracking antenna are displayed in Figures 14(a)–(b). The highest gain 5.82 dBi is obtained at a frequency of 2.80 GHz, and the minimum radiation efficiency of 80.2% is obtained at a frequency of 2.10 GHz with a gain value of 3.25 dBi.

Figures 15(a)–(d) show fabricated antenna, measurement setup using vector network analyzer, and anechoic chamber testing of the proposed antenna.

Figures 16(a)–(c) clearly indicate that simulated and measured results of the proposed antennas are in close agreement. Measured and simulated return losses and VSWRs shown in Figures 16(a) and (b) clearly show that the return loss and VSWR achieved at lower band at 1.46–1.73 GHz and upper band at 2.30–2.62 GHz are in acceptable range. Figure 15(d) indicates the setup of antenna under test (AUT) kept in an anechoic chamber for testing with a horn antenna. The better gain improvement can be achieved than simulated in measured gain results as shown in Figure 16(c). Figure 17 indicates the measured radiation pattern with a reflector structure which is close to the simulated results as mentioned in Figure 11.

3.9. Parameter Comparison of Like Antennas

The proposed GPS tracking wearable antenna is compared with the available existing similar antennas in Table 5 in terms of antenna performance parameters like substrate used, antenna gain, antenna size, -10 dB bandwidth, and SAR values.

It is noticed from the comparison table that the proposed antenna is compact with respect to designs shown [12–15, 18–20, 24, 26] except for [25], but as per dielectric constant of proposed antenna we tried to miniaturize structure. The simulated SAR values are compared with existing literature, and it is clearly indicated that the proposed antenna gives 0.01 W/kg and 0.02 W/kg values at lower and upper frequency bands which are not harmful to animals and $<$ 0.02 W/kg for 10 gm tissue. In some literature, detailed SAR analysis has not been analyzed [14, 18–20, 25]. The proposed antenna along with above mentioned importance shows CP which is the main requirement when antenna is used in forest or remote position for tracking applications with good axial ratio values as discussed in Figure 9. These parameters make the antenna suitable for Wi-Fi, ISM, WLAN, and wearable applications as well as for GPS/GNSS animal tracking applications and rescue searching and security operations.

4. CONCLUSIONS

The proposed dual-band CPW feed, strip-radiator, and reflector based multi-layered antenna, with circular polarization, offers a compelling solution for modern wireless communication needs. By leveraging the protruding inverted U-strip and semi-circular arc-strip design, the antenna efficiently covers the WLAN/ISM band (2.30–2.62 GHz) and GPS L1 band (1.46–1.73 GHz), ensuring versatile functionality across multiple frequency ranges. Impressively good FBR and low SAR values, below 0.01 W/kg at 1.60 GHz and below 0.02 W/kg at 2.41 GHz, underscore the antenna's commitment to minimizing electromagnetic exposure to human tissue, thus prioritizing user safety. With axial ratio findings indicating superior CP characteristics, the antenna attains values of 1.29 dB and 2.02 dB, both below the 3 dB threshold, ensuring high-quality signal reception across its operating bands.

REFERENCES

[1] Khaleel, H., *Innovation in Wearable and Flexible Antennas*, 2014.

[2] Paracha, K. N., S. K. A. Rahim, P. J. Soh, M. R. Kamarudin, K. G. Tan, Y. C. Lo, and M. T. Islam, "A low profile, dual-band, dual polarized antenna for indoor/outdoor wearable application," *IEEE Access*, 1–1, 2019.

[3] Pawase, T., A. Malhotra, and A. Mahajan, "Compact hybrid EBG microstrip antenna for wearable applications," *Frequenz*, Vol. 77, No. 11/12, 557–566, 2023.

[4] Pawase, T. N., A. Malhotra, and A. Mahajan, "Circularly polarized flexible dual-band microstrip antenna using Kapton material," *International Journal of Microwave & Optical Technology*, Vol. 17, No. 2, 149, 2022.

[5] Paracha, K. N., S. K. A. Rahim, P. J. Soh, M. R. Kamarudin, K.-G. Tan, Y. C. Lo, and M. T. Islam, "A low profile, dual-band, dual polarized antenna for indoor/outdoor wearable application," *IEEE Access*, Vol. 7, 33 277–33 288, 2019.

[6] Wang, J. J., "Antennas for global navigation satellite system (GNSS)," *Proceedings of the IEEE*, Vol. 100, No. 7, 2349–2355, 2012.

[7] Dierck, A., H. Rogier, and F. Declercq, "An active wearable dual-band antenna for GPS and iridium satellite phone deployed in a rescue worker garment," in *2013 IEEE International Conference on RFID-technologies and Applications (RFID-TA)*, 1–5, Johor Bahru, Malaysia, 2013.

[8] Ali, U., S. Ullah, B. Kamal, L. Matekovits, and A. Altaf, "Design, analysis and applications of wearable antennas: A review," *IEEE Access*, Vol. 11, 14 458–14 486, 2023.

[9] Varshney, A. and G. Rawat, "A microwave rectangular waveguide-to-microstrip line transitions@ 30 GHz," *International Journal of Emerging Technology and Advanced Engineering*, Vol. 3, No. 8, 563–568, 2013.

[10] Varshney, A., V. Sharma, C. Nayak, A. K. Goyal, and Y. Massoud, "A low-loss impedance transformer-less fish-tail-shaped MS-to-WG transition for K-/Ka-/Q-/U-band applications," *Electronics*, Vol. 12, No. 3, 670, 2023.

[11] Varshney, A., V. Sharma, I. Elfergani, C. Zebiri, Z. Vujicic, and J. Rodriguez, "An inline V-band WR-15 transition using antipodal dipole antenna as RF energy launcher @ 60 GHz for satellite applications," *Electronics*, Vol. 11, No. 23, 3860, 2022.

[12] Abirami, B. S. and E. F. Sundarsingh, "EBG-backed flexible printed Yagi–Uda antenna for on-body communication," *IEEE Transactions on Antennas and Propagation*, Vol. 65, No. 7, 3762–3765, 2017.

[13] Velan, S., E. F. Sundarsingh, M. Kanagasabai, A. K. Sarma, C. Raviteja, R. Sivasamy, and J. K. Pakkathillam, "Dual-band EBG integrated monopole antenna deploying fractal geometry for wearable applications," *IEEE Antennas and Wireless Propagation Letters*, Vol. 14, 249–252, 2014.

[14] Zhang, X., Z. Teng, Z. Liu, and B. Li, "A dual band patch antenna with a pinwheel-shaped slots EBG substrate," *International Journal of Antennas and Propagation*, Vol. 2015, No. 1, 815751, 2015.

[15] Yan, S., P. J. Soh, and G. A. Vandenbosch, "Low-profile dual-band textile antenna with artificial magnetic conductor plane," *IEEE Transactions on Antennas and Propagation*, Vol. 62, No. 12, 6487–6490, 2014.

[16] Paracha, K. N., S. K. A. Rahim, P. J. Soh, M. R. Kamarudin, K.-G. Tan, Y. C. Lo, and M. T. Islam, "A low profile, dual-band, dual polarized antenna for indoor/outdoor wearable application," *IEEE Access*, Vol. 7, 33 277–33 288, 2019.

[17] Joshi, R., E. F. N. M. Hussin, P. J. Soh, M. F. Jamlos, H. Lago, A. A. Al-Hadi, and S. K. Podilchak, "Dual-band, dual-sense textile antenna with AMC backing for localization using GPS and WBAN/WLAN," *IEEE Access*, Vol. 8, 89 468–89 478, 2020.

[18] Rojhani, N., S. S. Golazari, N. Amiri, and F. H. Kashani, "CPW-fed circular polarized square slot antenna for GPS applications," in *2018 IEEE International RF and Microwave Conference (RFM)*, 37–40, Penang, Malaysia, 2018.

[19] Yuan, J., Y. Li, Z. Xu, and J. Zheng, "A compact CPW-fed low-profile wideband circularly polarized slot antenna with a planar ring reflector for GNSS applications," *International Journal of Antennas and Propagation*, Vol. 2019, No. 1, 6463101, 2019.

[20] Mishra, S., S. Das, S. S. Pattnaik, S. Kumar, and B. K. Kanaujia, "Low-profile circularly polarized planar antenna for GPS L1, L2, and L5 bands," *Microwave and Optical Technology Letters*, Vol. 62, No. 2, 806–815, 2020.

[21] Singh, H., K. Srivastava, S. Kumar, and B. K. Kanaujia, "A planar dual-band antenna for ISM/wearable applications," *Wireless Personal Communications*, Vol. 118, 631–646, 2021.

[22] Gundapaneni, S., G. Raju, and A. S. D. Pendurthi, "Inverted Ω-shaped antenna for 2.45 GHz ISM band wearable applications," *Iranian Journal of Science and Technology, Transactions of Electrical Engineering*, Vol. 47, No. 3, 1177–1186, 2023.

[23] Balani, C. A., *Antenna Theory: Analysis and Design*, 2nd ed., Wiley, 1996.

[24] Ramli, M. N., P. J. Soh, H. A. Rahim, M. F. Jamlos, and F. N. Giman, "SAR for wearable antennas with AMC made using PDMS and textiles," in *2017 XXXIInd General Assembly and Scientific Symposium of the International Union of Radio Science (URSI GASS)*, Montreal, QC, Canada, 2017.

[25] Chandra, K., M. Kumar, and M. D. Upadhayay, "Triple band compact monopole antenna for applications like bluetooth, WiMax and WLAN," *IETE Journal of Research*, Vol. 69, No. 8, 5654–5669, 2023.

[26] Ni, A., W. Wang, J. Xue, Z. Wang, and L. Zhang, "A metasurface-based low-profile circularly polarized antenna with double-wide beam for global navigation satellite system," *Progress In Electromagnetics Research*, Vol. 144, 43–53, 2024.